



1

2 **Missing sea-level rise in southeast Greenland during and since**
3 **the Little Ice Age**

4

5 Sarah A. Woodroffe¹, Leanne M. Wake², Kristian K. Kjeldsen³, Natasha L.M. Barlow⁴, Antony J.
6 Long¹, Kurt H. Kjær⁵

7

8 ¹Department of Geography, Durham University, Lower Mountjoy, South Road, Durham, DH1 3LE,
9 UK, s.a.woodroffe@durham.ac.uk

10 ²Department of Geography and Environmental Sciences, Northumbria University, Ellison Place,
11 Newcastle upon Tyne, NE1 8ST, UK, leanne.wake@northumbria.ac.uk

12 ³Geological Survey of Denmark and Greenland (GEUS), 1350 Copenhagen K, Denmark, kkk@geus.dk

13 ⁴School of Earth and Environment, University of Leeds, LS2 9JT, UK, n.l.m.barlow@leeds.ac.uk

14 ⁵GeoGenetics, Globe Institute, University of Copenhagen, 1350 Copenhagen K, Denmark,
15 kurtk@sund.ku.dk

16 *Correspondence to:* Sarah A. Woodroffe (s.a.woodroffe@durham.ac.uk)

17

18 **Abstract**

19 The Greenland Ice Sheet has been losing mass at an accelerating rate over the past two decades.
20 Understanding ice mass and glacier changes during the preceding several hundred years, prior to
21 geodetic measurements, is more difficult because evidence of past ice extent in many places was later
22 overridden. Saltmarshes provide the only continuous records of Relative Sea Level (RSL) from close
23 to the Greenland Ice Sheet that span the period of time during and since the Little Ice Age (LIA) and
24 can be used to reconstruct ice mass gain and loss over recent centuries. Saltmarsh sediments collected
25 at the mouth of Dronning Marie Dal, close to the Greenland Ice Sheet margin in southeast Greenland,
26 record RSL changes over the past c. 300 years through changing sediment and diatom stratigraphy.
27 These RSL changes record a combination of processes that are dominated by local/regional changes in



28 Greenland Ice Sheet mass balance during this critical period that spans the maximum of the LIA and
29 20th Century warming. In the early part of the record (1725-1762 CE) the rate of RSL rise is higher
30 than reconstructed from the closest isolation basin at Timmiarmiut, but between 1762-1880 CE the RSL
31 rate is within the error range of rate of RSL change recorded in the isolation basin. RSL begins to
32 slowly fall around 1880 CE and then accelerates since the 1990s, with a total amount of RSL fall of
33 0.08 ± 0.1 m in the last 140 years. Modelled RSL, which takes into account contributions from post-
34 LIA Greenland Ice Sheet Glacio-isostatic Adjustment (GIA), ongoing deglacial GIA, the global non-
35 ice sheet glacial melt fingerprint, contributions from thermosteric effects, the Antarctic mass loss sea-
36 level fingerprint and terrestrial water storage, over-predicts the amount of RSL fall since the end of the
37 LIA by at least 0.5 m. The GIA signal caused by post-LIA Greenland Ice Sheet mass loss is by far the
38 largest contributor to this modelled RSL, and error in its calculation can have a large impact on RSL
39 predictions at Dronning Marie Dal. We cannot reconcile the modelled RSL and the saltmarsh
40 observations, even when moving the termination of the LIA to 1800 CE and reducing the post-LIA
41 Greenland mass loss signal by 30 %, and a ‘budget residual’ of ± 2.5 mm/yr since the end of the LIA
42 remains unexplained.

43

44 Keywords: Greenland, relative sea level, saltmarsh, glacio-isostatic adjustment, Little Ice Age, sea-level
45 budget

46

47 **1. Introduction**

48 Studies using a range of different geodetic methods all agree that the Greenland ice sheet (GrIS) has
49 been losing mass at an accelerating rate over the past two decades (Bevis et al., 2019, 2012; Chen et al.,
50 2021; Khan et al., 2015; Moon et al., 2012; Pritchard et al., 2009; The IMBIE Team, 2020; van den
51 Broeke et al., 2009). There is however less known about when and at what rate ice mass loss occurred
52 in Greenland during the last millennium until the start of the satellite and GPS eras, during periods of
53 climate warming and cooling (Briner et al., 2020; Khan et al., 2020; Kjær et al., 2022). Using Little Ice
54 Age (LIA) trimlines and stereo-photogrammetric imagery recorded between 1978-1987, Kjeldsen et al.
55 (2015) estimated an average Greenland-wide total ice mass loss of c. 75 Gt/yr during the 20th Century.
56 However, understanding how the rate of mass loss varied during the 20th Century is more complex



57 because it requires us to put a date on the end of the LIA, and to find a way of reconstructing mass loss
58 fluctuations without the help of continuous geodetic data. Understanding ice mass and glacier changes
59 during the preceding several hundred years is even more difficult because evidence of past ice sheet
60 extent in many places has been overridden by later advances (Briner et al., 2011; Kjær et al., 2022).

61

62 Salt marshes in nearfield settings record the timing and magnitude of fluctuations in ice mass during
63 the last few centuries through changes in relative sea-level (RSL) (e.g. Long et al., 2012). RSL reflects
64 the interplay of different cryosphere and oceanic processes but the dominant process close to an ice
65 sheet is the visco-elastic signature of local and regional mass changes through time (Farrell and Clark,
66 1976). Salt marshes form in the upper part of the intertidal zone and can continuously accumulate
67 organic sediment (Allen, 2000). Salt marshes in Greenland are generally small features with a very
68 short growing season, low sedimentation rates and may be affected by interactions with winter shore-
69 fast ice (Lepping and Daniëls, 2007). However, they can survive in these conditions and provide the
70 only continuous records of RSL from close to the GrIS that span the period during and since the LIA
71 and can be used to reconstruct ice mass gain and loss over recent centuries (Long et al., 2012, 2010;
72 Woodroffe and Long, 2009).

73

74 This study reports for the first time a continuous RSL record over the past ~300 years from a salt marsh
75 within 5 km of the ice sheet margin in southeast Greenland. The sediments and plant remains in the
76 marsh record RSL fluctuations over the last few hundred years and therefore provide a unique record
77 of changes in regional RSL during and since the LIA in Greenland. We predict local RSL changes by
78 creating a sea-level budget which includes predictions from a Glacio-Isostatic Adjustment (GIA) model
79 with c. 430 Gt ice mass loss in southeast Greenland between the end of the LIA and 2010 (as defined
80 by Kjeldsen et al., 2015), and estimates of other contributions since the end of the LIA including mass
81 loss from Greenland peripheral glaciers, non-Greenland ice, the thermosteric contribution and the effect
82 of terrestrial water storage in the 20th and 21st Centuries. Comparing the modelled sea-level budget and
83 the saltmarsh data provides an opportunity to consider potential errors in both methods and suggest how
84 we might bring model and data estimates closer together, as well as develop better understanding of the



85 nature of historical RSL in southeast Greenland and implications for coastline response to future,
86 enhanced GrIS and peripheral glacier melt.

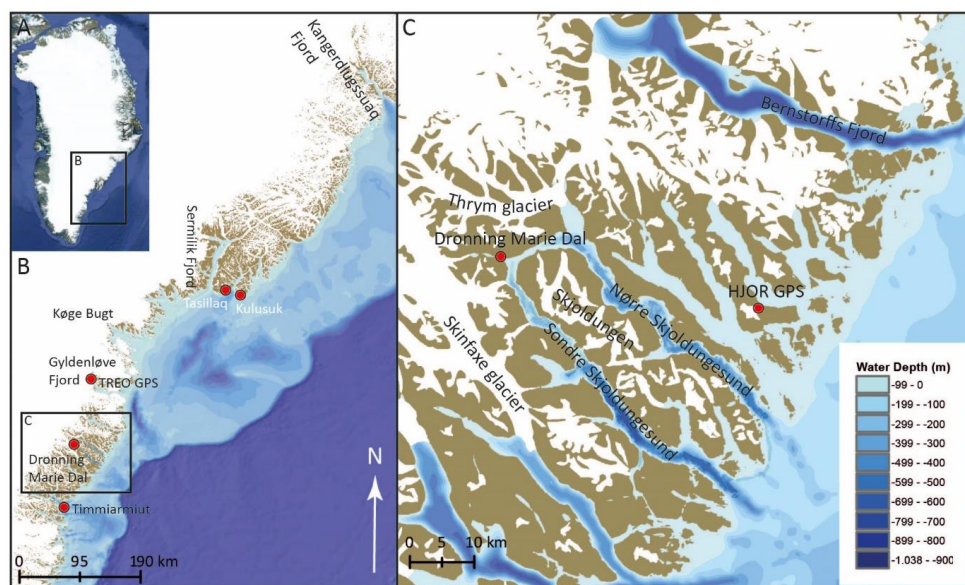
87

88 2. Study site and methods

89 2.1 Field site and glacial history of the region

90 The saltmarsh record is from 63.470°N, -41.925°W at the head of Dronning Marie Dal in southeast
91 Greenland (Figure 1A,B, Fig 2). The saltmarsh is fed by freshwater and sediment from Dronning Marie
92 Dal, a formerly glaciated valley that drains part of the nearby Skinfaxe outlet glacier. Dronning Marie
93 Dal is at the head of the 50 km long marine fjord Søndre Skjoldungesund which together with Nørre
94 Skjoldungesund encompass the glaciated island of Skjoldungen (Figure 1C). The northern fjord has a
95 bedrock sill mid-fjord at c. 215 m below sea level, while the southern fjord has a narrow central section
96 with a sill located at 77 m below sea level (Kjeldsen et al., 2017). The narrow stretch connecting the
97 two fjords at their inland extent is generally shallow, sheltering the salt marsh at Dronning Marie Dal.
98 The region is dominated by long, steep-sided marine fjords with the GrIS ending at the coast in marine-
99 terminating outlet glaciers.

100





101 *Figure 1. A) Map of Greenland © Google Earth, B) Southeast Greenland region showing the location*
102 *of the field site (Dronning Marie Dal) alongside other studied fjords, C) Dronning Marie Dal saltmarsh*
103 *at the head of Sondre Skjoldungesund, between the Skinfxaxe and Thrum glacier margins.*

104

105 Relatively little is known about the deglacial history of the southeast compared to the southwest of
106 Greenland. Most work has been undertaken in the large fjords (e.g. Kangerdlugssuaq, Sermilik, Køge
107 Bugt, Gyldenløve, Bernstorffs Fjord, Figure 1) to the north of the field area using ^{10}Be measurements
108 to reconstruct fjord deglaciation. During the LGM the ice sheet reached the shelf edge (50-80 km from
109 the outer coast) in this region and in the offshore Kangerdlugssuaq Trough to the north of the study area
110 the ice sheet started to retreat by c. 17 ka BP (Funder et al., 2011). Onshore deglaciation at the outer
111 coast occurred earlier to the north (Kangerdlugssuaq - 11.8 +/- 1ka BP) compared to the south
112 (Bernstorffs Fjord - 10.4 +/- 450 ka BP), driven by incursion of warm Atlantic water into the fjords
113 from the Irminger Current, moderated by local coastal bathymetry and atmospheric warming during the
114 early Holocene (Dyke et al., 2018, 2014; Hughes et al., 2012). ^{10}Be dates on boulders from outer and
115 inner Skjoldungesund suggest deglaciation here occurred in the early Holocene (inner fjord by 10.4
116 ± 0.4 ka BP) (Levy et al., 2020). Following retreat from the shelf edge, the deglaciation model HUY3
117 simulates retreat onshore by 10 ka BP, which largely agrees with the field evidence from
118 Skjoldungesund, with the ice sheet slightly inland of its LIA maximum position at 4 ka BP (Lecavalier
119 et al., 2014). The deglacial marine limit is low in this region (c. 20-40 m) suggesting less deglacial
120 mass loss compared to elsewhere in Greenland (Funder and Hansen, 1996). Observations of strandlines
121 up to 75 m above sea level in this region, reported by Vogt (1933) are cut into bedrock and are highly
122 unlikely to be of marine origin.

123

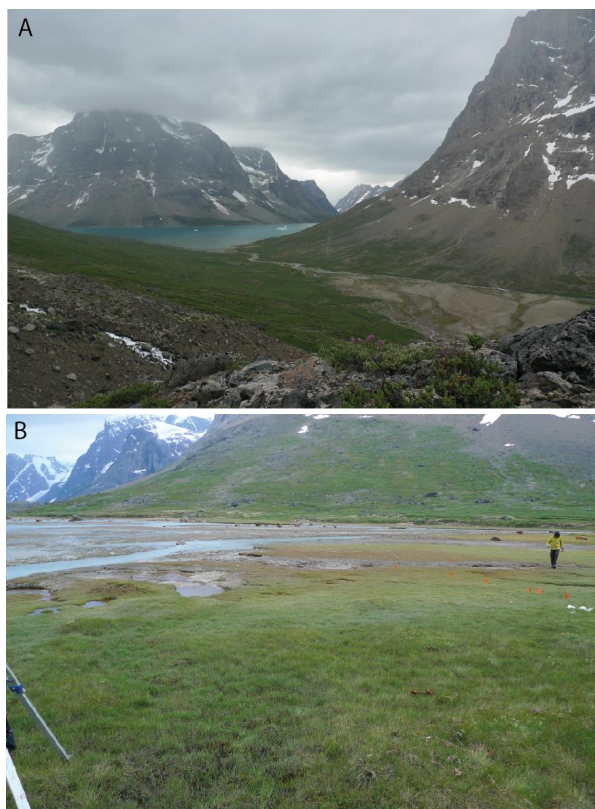
124 The HUY3 geophysical model predicts slight crustal subsidence at the coast today caused primarily by
125 a local late Holocene neoglacial readvance (resulting in RSL rise of 1-1.5 mm/yr over the last 1000
126 years) (Lecavalier et al., 2014). However, a recent GPS-derived GIA model (GNET-GIA) offers an
127 alternative solution with GIA uplift calculated at +2.8mm/yr and +3.1 mm/yr at nearby HJOR and
128 TREO GPS sites (Figure 1), which would result in pre-20th Century RSL fall at Dronning Marie Dal
129 (Khan et al., 2016). By comparing GPS data and absolute gravity observations over a 20-year period,



130 van Dam et al (2017) also suggest ongoing GIA uplift of $+4.5 \pm 1.4$ mm/yr at Kulusuk (300 km to the
131 north). These GIA estimates, based on modern observations, are corrected for elastic deformation in
132 response to modern mass balance changes to predict ongoing deglacial GIA. The most recent
133 examination of Greenland GIA model outputs and GPS data by Adhikari et al. (2021) suggests that
134 residual uplift caused by mass loss since the Medieval Warm Period, and in particular since the LIA,
135 accompanied by a reduced mantle viscosity on sub-centennial timescales, can explain the observed
136 discrepancy between uplift rates from HUY3 and elastic-corrected GPS uplift rates around Greenland.
137
138 LIA moraines are situated beyond the current frontal margins of the GrIS and local glaciers in this
139 region and demonstrate clearly that glacial retreat has occurred during the 20th Century (Bjork et al.,
140 2012). The instrumental temperature record from Tasiilaq indicates 2°C per decade of warming
141 between 1919 and 1932 CE (the early twentieth-century warming (ECW)), followed by cooling during
142 the 1950's to 1970's and steady temperature rise of 1.3°C per decade since 1993 (Bjork et al., 2012;
143 Chylek et al., 2006; Wood and Overland, 2010). Despite these decadal temperature fluctuations, and
144 the overall pattern of post-LIA retreat of southeast Greenland glaciers, the nearest glaciers to the field
145 site (Skinfaxe and Thrym, Figure 1C) have been relatively stable at their present positions since at least
146 the 1930s (Bjork et al., 2012). It is important to note however that Skinfaxe sits on a ledge in its fjord
147 system so would require significant thinning to dislodge it from its current position and Thrym Glacier
148 appears to be resting on shallow prograding bedrock (Bjork et al., 2012; Morlighem et al., 2017). The
149 total ice mass loss from the two drainage basins closest to the field site (Central East and South-East in
150 Kjeldsen et al., 2015) is 249 Gt between the end of the LIA and 1983, 134 Gt between 1983 and 2003
151 and 45 Gt between 2003 and 2010, based on the volume of loss from LIA trimlines and more recent air
152 photos. There is a significant increase ($\sim 70\%$) in the amount of regional mass loss during the post-1983
153 period compared to earlier in the 20th Century. We hypothesise that regional ice mass loss since the end
154 of the LIA should produce a visco-elastic GIA response recorded as variable 20th century RSL change
155 by local salt marsh sediments, such as those at Dronning Marie Dal (Figure 2).
156



157
158
159
160
161
162
163
164
165
166
167
168
169
170
171
172



173 *Figure 2. A) photograph looking East down the Dronning Marie Dal valley towards the head of Sondre*
174 *Skoldungesund and the salt marsh where the valley meets the fjord. B) photograph of the Dronning*
175 *Marie Dal salt marsh showing the low-angled relief of the marsh and zonation of salt marsh vegetation*
176 *(high marsh in the foreground).*

177

178 2.2 Reconstructing RSL using saltmarsh sediments

179 We collected salt marsh sediments by digging a small pit using a spade from the present-day high salt
180 marsh at the mouth of Dronning Marie Dal (Figure 1C, 2). The analysed sediment section is 13 cm
181 thick, with organic silt containing saltwater-tolerant diatoms situated over compacted sand-rich silt
182 where no diatoms are present (Figure 3). We sampled the fossil sediment section at 0.25 cm intervals
183 in the top 1 cm, and at 0.5 cm intervals further downcore to provide high-resolution RSL estimates,
184 bearing in mind the slow rate of sedimentation in most Greenlandic salt marshes (Long et al., 2012;
185 Woodroffe and Long, 2009). To reconstruct local RSL we investigated diatom assemblages across the



186 present-day salt marsh in the same location to understand changes in assemblages with elevation across
187 the upper part of the intertidal zone (Figure 3A). We then compared these assemblages to those found
188 through the sediment core using a visual assessment technique, that places weight on certain key taxa
189 that change abundance at clearly defined elevations (Long et al., 2012, 2010; Woodroffe and Long,
190 2009). The main species used to reconstruct RSL are the high marsh/freshwater species *Pinnularia*
191 *intermedia* and the high to low marsh species *Navicula cincta*. We prefer this method over a transfer
192 function approach (e.g. Barlow et al., 2013) because it relies on certain indicator species that occur at
193 narrowly defined levels, but also utilises other evidence such as vertical diatom succession and the
194 stratigraphy to interpret changes in RSL.

195

196 We initially calculated the elevations of modern and fossil saltmarsh samples to mean sea level (MSL)
197 using a high-precision dGPS. However due to technical issues with post-processing we instead rely on
198 tidal data from Timmiarmiut (100 km to the S) and tidal predictions from Tasiilaq (300 km to the NE)
199 collected during our fieldwork, along with knowledge about saltmarsh vegetation zonation in Greenland
200 and their general relationship to tidal levels, to relate fossil and modern saltmarsh elevations to mean
201 sea level (MSL). The tidal data from Timmiarmiut show that although the timing of daily tidal
202 fluctuations differs to predictions for Tasiilaq, the amplitude of tidal fluctuations is remarkably similar
203 (within 0.1 m). The tidal range (lowest to highest astronomical tide) at the outer coast is approximately
204 3.7 m. We have some confidence therefore that tidal predictions for Tasiilaq are applicable (with a time
205 correction) along the outer coast anywhere between Tasiilaq and Timmiarmiut, although the distances
206 involved are large. This leaves the issue of tidal range amplification or dampening in fjord-head settings
207 to consider, as the Dronning Marie Dal site is c. 50 km up-fjord from the open ocean (Figure 1C). This
208 is considered elsewhere in Greenland by Richter et al., (2011) who show that this effect is variable due
209 to fjord bathymetry and cross-section geometry, and ranges from -9 cm to +14 cm up fjord compared
210 to the fjord mouths on the west coast in fjords of similar length to Søndre Skoldungesund. Modern
211 saltmarsh vegetation at Dronning Marie Dal grows between 0.1 m above Highest Astronomical Tide
212 (HAT) and 0.08 m below Mean High Water of Spring Tide (MHWST) levels, which is very similar to
213 saltmarsh vegetation ranges we have observed elsewhere in southeast and southwest Greenland
214 (unpublished data and Woodroffe and Long, 2010, 2009). We are therefore confident that any effect of



215 the fjord-head setting on tidal range is small. We have not included an uncertainty estimate in our
216 overall RSL reconstruction to reflect this, because the uncertainty in the proxy elevations is already of
217 a similar magnitude (± 0.10 - 0.15 m, see Table S2 in Supplementary Information).

218

219 2.3 Chronology

220 To provide a chronology to constrain the timing of reconstructed RSL changes we use a range of
221 complementary methods to maximise the precision of the resultant age-depth model. Very low
222 concentrations of ^{210}Pb in the sediments required us to use other methods to provide recent
223 sedimentation rates. We investigated the presence of Total Mercury (Hg) (mg/kg, which includes both
224 mineral and atmospheric deposition) within the sediments using acid dissolution and quadrupole ICP-
225 MS as an indicator of anthropogenic emissions. Other studies in western and northern Greenland note
226 that between 1850-1900 CE there is more than a 2-fold increase in abundance of total Hg in lake
227 sediments compared to late Holocene levels (Bindler et al., 2001; Lindeberg et al., 2006; Shotyk et al.,
228 2003; Zheng, 2015), whereas Perez-Rodriguez et al. (2018) see a rapid increase in Hg abundance from
229 1880 onwards in southern Greenland. We therefore assume that the onset of detectable Hg above
230 background level in the Dronning Marie Dal saltmarsh sediments at 4-4.5 cm indicates an age of 1850-
231 1900 CE and use 1875 ± 25 CE in the age-depth modelling described below. For the earlier part of the
232 sediment record we submitted seeds and leaves from saltmarsh and nearby freshwater plants picked
233 from multiple horizons within the sediment for AMS ^{14}C dating at the $^{14}\text{Chrono}$ centre at Queen's
234 University, Belfast (Table 1). We generated an age-depth model for the whole sequence using the
235 *P_Sequence* approach with *variable k* in Oxcal v. 4.3 using the IntCal20 calibration curve (Bronk
236 Ramsey, 2009; Ramsey and Lee, 2013; Reimer et al., 2020). The resultant age-depth model uses the
237 Hg chronohorizon (1850-1900 CE) and three ^{14}C dates from lower in the sequence to estimate the age
238 of every 0.25 cm of sediment in the sediment section with associated uncertainty (Table 1 and Table S2
239 in supplementary information). The chronological uncertainty reported throughout this study is the
240 95% probability distribution (Bronk Ramsey, 2009).

241

242 We exclude the ^{14}C ages at 6-6.5 cm (UBA28477) and 9-9.5 cm (UBA28478) from the age-depth model
243 because they were on extremely small samples (< 0.8 mg carbon) and are from samples that mix seeds



244 and leaves from high salt marsh with freshwater plants that would not have been growing close together
 245 at the time (based on the palaeoenvironment recorded by the fossil diatom assemblage, and the
 246 distribution of diatoms and vegetation types on the present-day saltmarsh) (Table 1). The dated
 247 macrofossils from lower in the sequence are more likely to be autochthonous as the diatoms record a
 248 high marsh to freshwater environment, close to HAT, at the time of deposition.
 249

Core depth (cm)	Lab number	¹⁴ C age (yr CE/BP)	¹⁴ C age error (yr/1 sigma)	F ¹⁴ C	F ¹⁴ C error	Cal curve	Dated material	Used in age model?
6-6.5	UBA28477	496 CE	508	1.0265	0.1421		Carex subspathacea seeds/Empetrum nigrum leaves	N
9-9.5	UBA28478	1955 CE	1	1.0107	0.0052		Carex subspathacea seeds/Empetrum nigrum leaves	N
10-10.5	UBA28481	208 BP	67	n/a	n/a	INTCAL20	Carex subspathacea seeds	Y
11.5-12	UBA28476	134 BP	93	n/a	n/a	INTCAL20	Carex subspathacea seeds	Y
12-13	UBA28479	44 BP	45	0.99453	0.00555	INTCAL20 + NHZ1	Carex subspathacea seeds	Y

250 *Table 1. Radiocarbon dated samples from the Dronning Marie Dal saltmarsh core.*

251

252 2.4 Modelling RSL

253 2.4.1 Deglacial RSL change

254 There is a high degree of uncertainty on the rate of GIA in south-east Greenland, owing largely to the
 255 lack of Holocene RSL data points to constrain deglacial history. Marine ingressions into an isolation
 256 basin at Timmiarmiut (100 km SW of Dronning Marie Dal) at c. 1140 CE (Table 2, also see Figures
 257 S1, S2 and Table S1 in the supplementary information) gives an empirical estimate of regional GIA and
 258 suggests that the linear rate of background RSL change over the past millennium is in the range of +0.2
 259 to +0.8mm/yr (Table 2). We therefore use a mid-point value of +0.5 mm/yr as the rate of RSL change
 260 due to ongoing deglacial GIA in this study, rather than model predictions outlined in Section 2.1 which
 261 are not validated using RSL data from this region.

262



263 *Table 2. Isolation basin sea-level index point from Timmiarmiut used to calculate the rate of RSL due*
264 *to ongoing GIA in this study.*

Location (lat,lon)	Sill height (m MTL)	Reference Water Level	RSL (m)	Max cal age CE	Min cal age CE	Cal age error +/-	¹⁴ C age	Lab code
Timmiarmiut XC1403A (62.4987, -42.2577)	1.33 +/- 0.5	Ingression (MHWST to HAT)	-0.24 +/- 0.5	1044	1243	99.5	873 +/- 30	AAR 25631

265

266 2.4.2 Post Little Ice Age Greenland contribution

267 The post-LIA contribution to RSL at Dronning Marie Dal is computed using the sea level algorithm of
268 Kendall et al. (2005) computerised by Milne and Mitrovica (2003). This code computes the geoidal and
269 crustal response to ice and ocean loads on a spherically-symmetric Earth discretized into 25 km-thick
270 elastic layers as defined by Dziewonski and Anderson (1981), and three viscous layers comprising a
271 lithosphere, upper and lower mantle. Lithospheric thicknesses (L) in the range 71-120 km are
272 considered, with upper mantle (ν_{UM}) and lower mantle (ν_{LM}) viscosities of $0.1-1 \times 10^{21}$ and $1-50 \times 10^{21}$
273 Pa s explored to quantify the effect on predicted RSL change of different assumptions about Earth
274 viscosity structure. The post-LIA ice history for the GrIS is derived from Kjeldsen et al. (2015) who
275 used a collection of aerial imagery from 1978-1987 CE to compare to historical trimlines assumed to
276 be indicative of a maximum LIA position of the ice sheet and use 1900 CE as a Greenland-wide year
277 of retreat from the maximum position, while acknowledging considerable local and regional
278 differences. The extrapolation method of point-scale changes in ice thickness over this time period to
279 the rest of the Greenland Ice Sheet is detailed in the methods section of Kjeldsen et al. (2015).

280

281 2.4.3 Contribution from Greenland glaciers

282 Changes in ice thickness in peripheral Greenland glaciers is determined in exactly the same way as the
283 post-LIA Greenland contribution. The peripheral Greenland glacier mass balance history is extracted
284 from Marzeion et al. (2015) and considered separately from the global glacier dataset (Section 2.4.4)
285 due to their proximity to the field site; the RSL response is computed as described in Section 2.4.2.

286

287 2.4.4 Contribution from global glaciers



288 We calculate the sea level contribution from global glaciers by first computing the global fingerprint
289 for a +1mm/yr barystatic contribution from glacier complexes defined in Marzeion et al. (2015, 2012)
290 since 1902. For the purposes of this calculation, we distribute the mass change across the glacierised
291 regions equally since the use of a 512 harmonic truncation masks sub 100 km-scale variability in ice
292 thickness change across regions outside of Greenland. Ice thickness change will vary internally to each
293 glacierised area, but the great distance between southeast Greenland and many of the sources of melt
294 means that the solution is insensitive to spatially inhomogeneous changes in ice thickness within the
295 source regions. Ice thickness changes for each of the global glacier complexes are discretized into
296 decadal loading intervals and the global sea level response is computed using the density configuration
297 in the Preliminary Reference Earth Model (PREM) (Dziewonski and Anderson, 1981). We use a
298 lithospheric thickness of 96 km to represent a global average applied to all glacial sites and omit the
299 viscous component from this calculation. Dronning Marie Dal is proximal to glacier sources in Iceland
300 and Baffin Bay so should display some level of sensitivity to ice loss distribution over these glacierised
301 areas. However, it is in the ‘near field’ with respect to both of these sites, and therefore the use of a
302 more realistic ice loss distribution in these areas (e.g. peripheral thinning) will reduce the relative sea-
303 level rise recorded in southeast Greenland. The influence of low-latitude glaciers is excluded from the
304 sea level fingerprint calculations, as the areas of mass loss are below the spatial resolution of the
305 fingerprinting code. This simplified method produces similar results that of Frederikse et al. (2020).

306

307 2.4.5 Contribution from the Antarctic Ice Sheet

308 Loss of ice mass from either East or West Antarctic Ice Sheets will produce a relatively uniform sea-
309 level change fingerprint over the northern Hemisphere (Bamber and Riva, 2010; Mitrovica et al., 2001).
310 Recent Antarctic Ice Sheet change (1992-present) is relatively well-documented and quantified
311 (Meredith et al., 2019) compared to the period represented by the RSL data in this study. However, a
312 recent study by Frederikse et al. (2020) that applied a Monte Carlo approach to balance the budget of
313 global sea-level rise since 1900 used estimates of 20th century Antarctic Ice Sheet mass balance obtained
314 from Adhikari et al. (2018) where the focus of mass loss throughout the 20th century is thought to be in
315 the West Antarctic Ice Sheet, amounting to a global sea-level change of 0.05 ± 0.04 mm/yr. We use the



316 resulting ensemble from Frederikse et al's (2020) analysis to compute Antarctic Ice Sheet contribution
317 at Dronning Marie Dal.

318

319 2.4.6 Contribution from steric changes

320 To compute the contribution from salinity and temperature changes in the nearby ocean, the
321 Thermodynamic Equation of Sea Water (McDougall and Barker, 2011) (algorithm available here:
322 <https://www.teos-10.org/>) was applied to compute the steric height of the ocean. This uses a suite of
323 proximal monthly temperature-depth and salinity-depth profiles extracted from the CMIP6 database for
324 the 'historical' experiments covering the period 1850-2014. The 'historical' experiment was chosen to
325 produce timeseries of depth-dependant potential temperature and salinity because the experiment forms
326 part of the principal set of CMIP6 simulations, and the forcing datasets provided to the AOGCMs are
327 consistent with a set of atmospheric and ocean observations (Eyring et al., 2016). We use only one
328 configuration of the variant ID, which relates to initialisation time and procedure, specific model
329 physics and forcing (r1i1p1f1) across all AOGCMs considered (NASA-GISS-E2, CESM2, AWI,
330 CanESM5 and FGOALS). The model output from the CMIP6 database has a spatial resolution in the
331 range of 50-200 km, so we use profiles located within 300 km of Dronning Marie Dal to calculate an
332 average trend in steric height for the nearby ocean. The steric heights are computed to reference depth
333 levels of 500 m, 1000 m, 2000 m and 3000 m. Computing steric heights to different reference levels
334 allow us to determine which depth(s) in the ocean are contributing to steric height variability. Ivchenko
335 et al. (2008) determined that for the North Atlantic for the period 1996-2006, applying a reference level
336 of 1000-1500 m was sufficient to capture steric height variability, although this study provides trends
337 in steric height across the maximum depth level available by each model in the region proximal to
338 Dronning Marie Dal.

339

340 2.4.7 Terrestrial Water Storage

341 To estimate the contribution of changes in terrestrial water storage we utilise the ensemble of timeseries
342 of Frederikse et al. (2020) covering the time-period 1900-2018 CE. This dataset was compiled by
343 including the effects of natural variability in water reservoirs attributed to hemispheric-scale
344 atmospheric and ocean circulation changes (Humphrey and Gudmundsson, 2019), changes in storage



345 from dam building (Chao et al., 2008) and groundwater depletion activities (Döll et al., 2014; Wada et
346 al., 2016).

347

348 In the next section the results from the field work, RSL reconstruction and sea-level modelling are then
349 compared to better understand changes in mass balance and RSL over recent centuries in southeast
350 Greenland.

351

352 **3. Results**

353 *3.1 Modern diatom assemblages*

354 Diatoms are zoned by elevation across the upper part of the intertidal zone at Dronning Marie Dal, with
355 individual species providing useful information for reconstructing RSL. Above 2.2 m MTL (>0.34 m
356 above HAT) no diatoms were found in surface sediments, probably because the environment is too arid.

357 There is a distinctive assemblage containing *Pinnularia intermedia* (>10 % at HAT, increasing to ~55
358 % in the highest samples) which ends at 2.2 m MTL. We use this as a proxy sea level indicator and to
359 reconstruct palaeo-marsh surface elevation changes when we find >10 % of *Pinnularia intermedia* in
360 fossil counts (Figures 3A and B and Table S2 in supplementary information). We find this upper
361 intertidal/supratidal *Pinnularia intermedia* assemblage at every marsh we have studied in southeast and
362 southwest Greenland and use it to reconstruct RSL rather than using a transfer function approach as its
363 precision is as good as or better (*Pinnularia intermedia* is present in >15 marshes between 59° and 69°
364 N in southwest and southeast Greenland with a vertical range of 0.2-0.4 m; unpublished data and Long
365 et al., 2012, 2010; Woodroffe and Long, 2010, 2009). Where *Pinnularia intermedia* is <10 % in fossil
366 sample assemblages we consider other species, particularly *Navicula cincta* which is present in greatest
367 abundance in lower parts of the marsh, to reconstruct RSL (Table S2 in supplementary information).

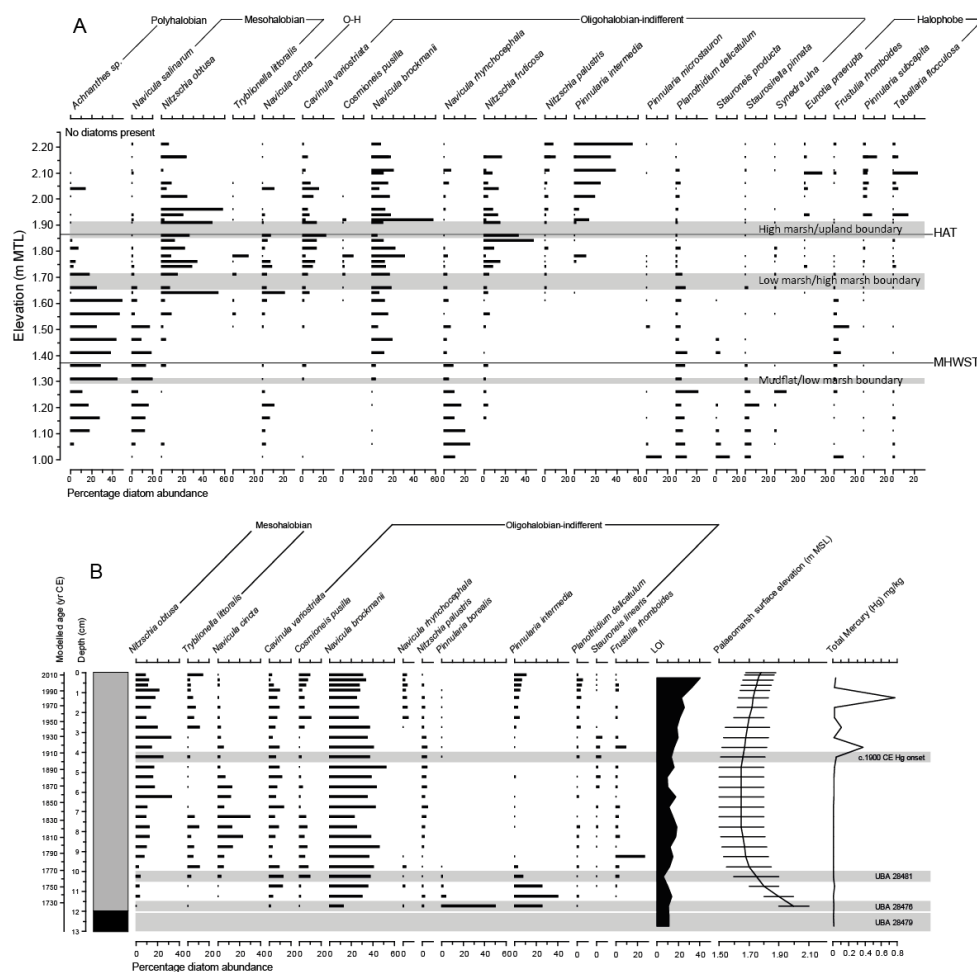
368

369 *3.2 Core stratigraphy and biostratigraphy*

370 The core stratigraphy consists of a compacted basal freshwater organic silt-clay, grading upwards into
371 organic high saltmarsh sediments, and then into a slightly silt-rich organic low salt marsh towards the
372 surface, with an increase in LOI values in the top 2 cm (Figure 3B). Diatoms are well preserved in the
373 core and show a trend of falling palaeo-marsh surface elevation upwards from the base of the sequence



374 as *Pinnularia intermedia* declines and *Navicula cincta* increases in abundance. In the top 3 cm
 375 *Pinnularia intermedia* increases in abundance recording RSL beginning to fall and palae-marsh
 376 surface elevation increasing (Figure 3B).
 377



378
 379 *Figure 3. A) Modern diatom data from the marsh at Dronning Marie Dal. Data are expressed as %*
 380 *total diatom valves (%TDV). Only data >10% TDV are shown. B) Fossil diatom counts, palae-marsh*
 381 *surface elevation reconstruction and total Mercury measurements from the Dronning Marie Dal*
 382 *saltmarsh core. Diatoms are expressed as a %TDV and only taxa with >10% TDV are shown.*
 383 *Stratigraphy is show in lefthand box where grey = saltmarsh sediment, black = freshwater peat. Total*
 384 *Mercury (mg/kg) was measured on salt marsh sediment using quadrapole ICP-MS.*

385



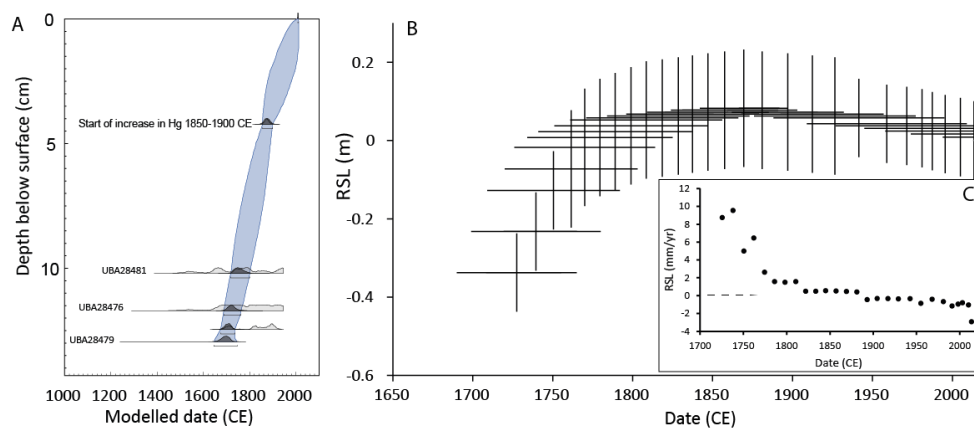
386 3.3 RSL reconstructions

387 The saltmarsh sediments and diatoms indicate long term RSL rise. The rate of RSL rise at the start of
388 the record (+8-13 mm/yr between 1725-1762 CE; Figures 4B and C) is significantly higher than the
389 rate reconstructed from the closest isolation basin at Timmiarmiut (+0.2-0.8 mm/yr; Table 2). This may
390 be due to LIA ice growth, including the glacier arm delivering sediment-laden meltwater to Dronning
391 Marie Dal, causing local ice loading and rapid infilling of accommodation space and salt marsh
392 development. The rate of RSL rise declines rapidly over the period 1762-1880 CE and is within the
393 error range of the isolation basin rate during most of this period (+0.3-3 mm/yr). This trend of rapid
394 and then slowly rising RSL between 1725-1880 CE is likely due to changes in the local LIA ice load
395 over this time period combined with ongoing millennial-scale GIA. The HUY3 model predicts +1.44
396 mm/yr of RSL rise over the past 1000 years in this region (Lecavalier *et al.* 2014) which is the same
397 sign as the salt marsh and isolation basin RSL data during this period. Other recent estimates of
398 centennial-scale GIA (Khan *et al.*, 2016; van Dam *et al.*, 2017) suggest that RSL should have been
399 falling over the past few hundred years at Dronning Marie Dal. The isolation basin and salt marsh data
400 instead suggest that RSL was rising or close to stable from c. 1100 CE until c. 1880 CE.

401

402 Since 1880 CE RSL began to fall, which is indicated clearly in the diatom record by the reintroduction
403 and increasing abundance up core of *Pinnularia intermedia*, a high marsh diatom species (Figure 3B).
404 This high marsh environment gives the most precise RSL reconstructions and therefore we have the
405 most confidence in the pattern of RSL during this recent part of the record. RSL began to fall around
406 1880 CE at a relatively constant rate (< -1mm/yr) until the 1990s, when the rate of fall accelerates to
407 between -1 and -3 mm/yr to present (2014 CE), resulting in a total amount of RSL fall of -0.08 ± 0.1 m
408 since 1880 CE (Figures 4B and C, Table 3, Table S2 in supplementary information).

409



410

411 *Figure 4A) age-depth model using three ¹⁴C ages and the Hg chrono-horizon, B) Dronning Marie Dal*
412 *RSL curve, C) rates of RSL change through time inferred from the RSL and age data.*

413

414 3.4 Modelled RSL changes

415 Published calculations of post LIA Greenland mass loss and other RSL contributors start at 1900 CE
416 (e.g. Kjeldsen et al., 2015; Marzeion et al., 2015), so we focus on this part of the salt marsh RSL record
417 to compare the reconstructed RSL with a modelled sea-level budget. The different contributions to the
418 sea-level budget are summarised in Table 3 and Figure 5. For an average Earth model configuration of
419 $L = 96\text{km}$, $\nu_{UM} = 0.5 \times 10^{21} \text{ Pa s}$ and $\nu_{LM} = 10 \times 10^{21} \text{ Pa s}$, post-LIA ice mass loss (from the GrIS only)
420 resulted in sea level change of -5.9 mm/yr at Dronning Marie Dal between 1900-2010. Between 1983-
421 2010 the modelled RSL rate was -10.1 mm/yr . Any chosen Earth configuration within the parameter
422 range explored does not significantly affect the predicted sea-level change; for 1900-2010, the range of
423 RSL fall was between -6.7 to -5.8mm/yr and 1983-2010 between -11.7 to -9.9 mm/yr . The contribution
424 of peripheral Greenland glaciers to RSL was on average $-1.7 \pm 0.2 \text{ mm/yr}$ between 1903 and present
425 day; with decadal-scale contributions of -3 to -5 mm/yr between 1923 and 1943. Global glacier mass
426 loss contributes $+0.24 \pm 0.06 \text{ mm/yr}$ RSL rise between 1903-2009. Antarctica has contributed more
427 significantly to sea-level change in recent years; for the period 1992 to 2016, the Antarctic Peninsula
428 and the West Antarctic Ice Sheet are thought to have resulted in $+0.06 \pm 0.73 \text{ mm/yr}$ of barystatic sea-
429 level change (Meredith et al., 2019). However, for the period 1850-2014 Frederikse et al. (2020)
430 compute $+0.08 \pm 0.08 \text{ mm/yr}$, rising to $+0.2\text{mm/yr}$ between 1970-2018.

431



432 The range of values for the modelled steric contribution are in Table 4. They represent an upper estimate
 433 of the magnitude and range of the steric component as only profiles showing significant RSL trends are
 434 used when calculating the mean. From 1850-2014, trends in steric height are in the range -0.23 to
 435 $+0.18$ mm/yr for a reference depth level of 1000 m and -0.36 to $+0.28$ mm/yr over a depth range of
 436 2000 m. An observation-based analysis of trends in steric height by Frederikse et al. (2020) shows the
 437 steric contribution from the upper 2000m of the ocean close to Dronning Marie Dal between 1957-2018
 438 is $+0.13$ mm/yr (we include steric trends derived for the period 1950-2014 in Table 4 for comparison).
 439 All models considered in Table 4 have larger values than Frederikse et al. (2020)'s estimates. Finally,
 440 the impact of terrestrial water storage amounts to a sea level fall of -0.13 ± 0.06 mm/yr at Dronning
 441 Marie Dal over the 20th century.

442

443 The different contributions to RSL are summed and plotted alongside the saltmarsh RSL data in Figure
 444 5. The sum of components predicts RSL fall of between 0.58-0.93 m since 1900 CE. This prediction
 445 is dominated by the contribution of GIA caused by post LIA Greenland and peripheral glacier mass
 446 loss, which is only counteracted a little by the other components which mostly predict small amounts
 447 of RSL rise. The saltmarsh data only reconstruct $\sim 0.08 \pm 0.1$ m of RSL fall since 1880 CE producing a
 448 large mismatch between the sea-level budget and the saltmarsh RSL data. However the RSL data does
 449 show an acceleration in the rate of RSL fall since the 1990s which agrees with accelerated GrIS mass
 450 loss in the 1983-2003 and 2003-2010 time periods in Kjeldsen et al. (2015).

451

452 *Table 3. Calculated amounts and rates of RSL change from the various contributors to the RSL budget*
 453 *at Dronning Marie Dal. Rates of RSL change are supplied with ± 2 -sigma uncertainty unless specified:*
 454 ** uncertainty reflects assumed $\pm 10\%$ error on rates which is larger than ± 2 -sigma. ** steric sea level*
 455 *contribution calculated from the average of significant trends for the 0-2000m depth interval from three*
 456 *models in Table 4. *** GIA from nearby isolation basin ingression with uncertainty calculated from*
 457 *upper and lower elevation reconstruction uncertainties.*

Contribution to sea-level budget	Local or global	Time period	Contribution to RSL change (mm), upper and lower estimates	Rate of RSL change (mm/yr) assumed for common period of 1900-2012
----------------------------------	-----------------	-------------	--	---



			calculated for common period of 1900-2012	
GIA caused by post LIA ice mass loss*	Local	1900-2010	-724, -593	-5.9 ± 0.6
GIA caused by Greenland peripheral glacier mass change*	Local	1903-2012	-202, -166	-1.7 ± 0.2
Millennial-scale deglacial GIA***	Local	1900-2018	33, 88	+0.5 ± 0.3
Local total				-7.1 ± 0.6 mm/yr
Global glaciers	Global	1903-2012	20, 33	+0.24 ± 0.06
Antarctica	Global	1900-2018	0, 18	+0.08 ± 0.08
Steric**	Global	1850-2014	-39, 39	+0.00 ± 0.35
Terrestrial water storage	Global	1900-2018	-21, -8	-0.13 ± 0.06
Global total				+0.19 ± 0.35 mm/yr
Total modelled RSL change at Dronning Marie Dal 1900-2012 (see Figure 5)			-933, -589	-6.9 ± 1.5 mm/yr
Rate of RSL change from saltmarsh data (1880-2014)				-0.67 ± 1.7 mm/yr

458

459

460 *Table 4: Mean trends in steric height anomalies for three reference levels (500, 1000 and 2000m)*

461 *calculated from profiles within 300km of Dronning Marie Dal using five models participating in the*

462 *CMIP6 analysis. In all cases, experiment variant ID was r1i1p1f1. Numbers in brackets denote number*

463 *of profiles displaying significant trends in steric height from which the mean and 2-sigma trends were*

464 *calculated. The AWI model produced no significant trends for either time-period whilst GISS-E2 did*

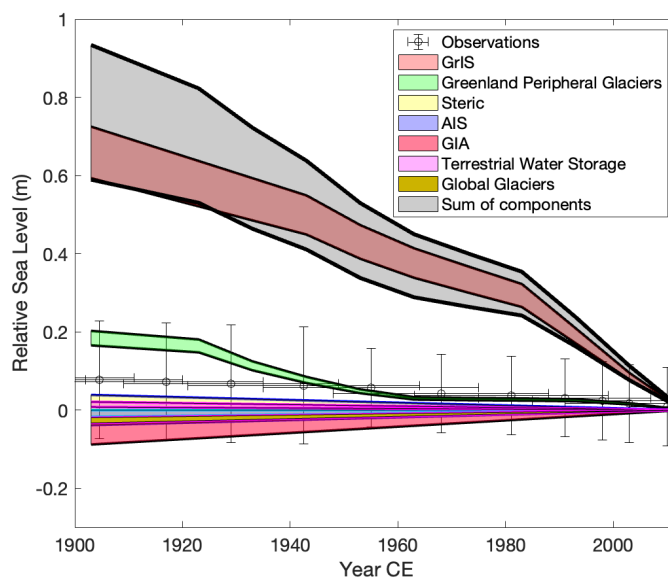
465 *not produce significant trends for 1850-2014.*

466

Model ID	Resolution (space)	Resolution (time)	0-500m	0-1000m	0-2000m
1850-2014					
GISS-E2	200km	Monthly	-	-	-
CESM2	100km	Monthly	0.08 ± 0.01 (34)	0.17 ± 0.01 (26)	0.09 ± 0.01 (7)
FGOALS	100km	Monthly	0.14 ± 0.12 (7)	0.18 ± 0.16 (11)	0.28 ± 0.04 (6)
AWI	25km	Decadal	-	-	-
CanESM5	100km	Monthly	-0.12 ± 0.1 (13)	-0.23 ± 0.08 (13)	-0.36 ± 0.06 (13)
1950-2014					
GISS_E2	200km	Monthly	0.17 ± 0.02 (10)	0.36 ± 0.03 (6)	0.75 ± 0.05 (3)
CESM2	100km	Monthly	0.63 ± 0.15 (37)	1.3 ± 0.11 (26)	1.24 ± 0.07 (7)
FGOALS	100km	Monthly	0.43 ± 0.17 (11)	0.57 ± 0.18 (12)	0.81 ± 0.15 (6)
AWI	25km	Decadal	-	-	-
CanESM5	100km	Monthly	0.97 ± 0.34 (15)	1.1 ± 0.32 (13)	0.96 ± 0.2 (8)

467

468



469

470 *Figure 5: Observed and modelled relative sea level change from 1900-2010 CE as a function of recent*
471 *and late Holocene Greenland ice thickness changes (GIA caused by the GrIS, Greenland peripheral*
472 *glaciers and millennial-scale GIA; the 'local' signal) and from sources outside of Greenland (steric*
473 *signal, AIS, terrestrial water storage and global glaciers). The sum of the modelled components is*
474 *shown as the grey shaded area and the GrIS and peripheral glacier contributions are shown with an*
475 *estimated $\pm 10\%$ uncertainty. The black crosses are the salt marsh-based RSL reconstruction.*

476

477 **4. Discussion**

478 The dominant contributors to post-LIA RSL change at Dronning Marie Dal are the adjustment of the
479 solid Earth and changes in geoid height in response to both post-LIA and millennial-scale Greenland
480 ice sheet changes. These contributors (ongoing GIA from the last deglaciation, post LIA Greenland
481 mass balance and mass loss from peripheral Greenland glaciers) amount to a modelled sea-level fall of
482 -7.1 mm/yr between 1900-2010. By contrast, the RSL contributors unrelated to cryospheric change in
483 Greenland only amount to modelled sea-level rise of $+0.19$ mm/yr, giving a total RSL fall of -6.9 mm/yr
484 between the end of the LIA and present (Table 3). This clearly does not fit with the observations from
485 the salt marsh data (Figures 4B, 5), which suggests that the rate of RSL fall between 1900-2013 is –
486 0.67 ± 1.7 mm/yr.



487

488 *4.1 Timing of the end of the LIA and Greenland ice sheet and peripheral glacier contribution*

489 To try to bring the post-LIA sea-level budget closer to the salt marsh observations, we explore two
490 possible sources of uncertainty in the dominant post LIA Greenland signal: 1) timing of the start of
491 post-LIA mass loss in Greenland and 2) greater uncertainty in modelled sea level associated with post-
492 LIA GrIS and peripheral glacier mass loss.

493

494 To explore the possibility that the total post-LIA Greenland mass loss occurred over a longer time period
495 we create four scenarios where the LIA maximum ice termination in Greenland is adjusted to begin at
496 1750, 1800, 1850 and 1900 CE, and the rate of mass loss is scaled accordingly with the end point
497 remaining at 2010 (as in Kjeldsen et al., 2015). We know that the LIA ice sheet response was different
498 around Greenland with multiple advance phases forced by different driving mechanisms, and it is
499 simplistic to suggest that the whole of the ice sheet began to lose mass simultaneously at 1900 CE (Kjær
500 et al., 2022), albeit it may serve as a Greenland-wide year. By adjusting the LIA termination date (and
501 therefore the start of Greenland and peripheral glacier mass loss) we can investigate the impact of earlier
502 ice retreat on RSL at Dronning Marie Dal. In this sensitivity analysis we recognise that moving the
503 LIA termination date in our modelling means that we are assuming the LIA ended simultaneously earlier
504 around the whole of Greenland, which is no more nuanced than assuming LIA termination at 1900 CE.
505 We also note that the glaciers closest to Dronning Marie Dal appear to have been at their LIA maximum
506 position in the early 20th Century, which does not agree with an earlier LIA end in this location (Bjork
507 et al., 2012), and a recent alkenone-based sea-surface temperature reconstruction from Nørre
508 Skjoldungesund suggests considerable warming here occurred late, between c. 1915-1945 CE
509 (Wangner et al., 2020). The analysis does however allow a first-order investigation into the sensitivity
510 of modelled post-LIA sea level to the length of time over which the post-LIA mass loss occurred.

511

512 The second parameter that we vary as part of this sensitivity study is the total amount of post-LIA mass
513 loss from the GrIS and peripheral glaciers, by assuming an error of up to -30% on these calculations.
514 Kjeldsen et al. 2015 report uncertainties in their mass loss estimates for the Southeast sector of the ice



515 sheet between 7-15 %, and so this sensitivity analysis allows us to test the effect on RSL at Dronning
516 Marie Dal of a smaller amount of mass loss since the end of the LIA in this region.

517

518 Varying both LIA termination date and total post LIA mass loss from the GrIS and peripheral glaciers
519 has a large effect on how much sea-level change from other components is required to close the post-
520 LIA budget (Figure 6). The ‘budget residual’ in Figure 6 refers to the misfit in mm/yr between the RSL
521 change reconstructed by the saltmarsh data and RSL change predicted by the sea-level budget
522 calculations. In essence this is the amount of sea-level change that we still need to ‘find’ to close the
523 budget even after we modify the timing and total amount of mass loss from the dominant contributors
524 to RSL change of GrIS and peripheral glacier retreat since the end of the LIA.

525

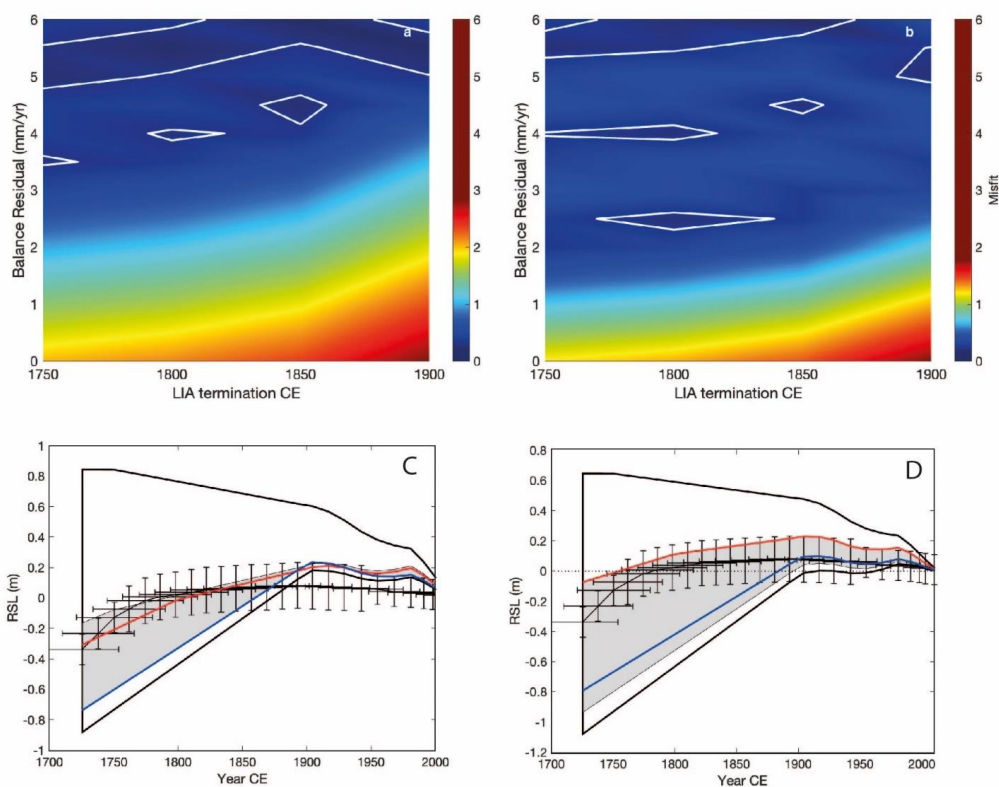
526 The time-period over which post LIA mass loss occurs is important for understanding the degree of
527 volume mismatch between the RSL observations and modelled contributions from the maximum extent
528 to present. Figure 6a indicates that moving the LIA termination date from 1900 CE to 1750 CE reduces
529 the ‘budget residual’ required to fit the RSL data from $\sim+5.5$ to $\sim+3.5$ mm/yr. This residual is reduced
530 further (to $\sim+2.5$ mm/yr) when considered alongside a 30% reduction in the amount of mass loss from
531 the GrIS and peripheral glaciers compared to volumes reconstructed by Kjeldsen et al. 2015 (GrIS) and
532 Marzeion et al. 2015 (peripheral glaciers) (Figure 6b). Figures 6c and d further illustrate these results.
533 Figure 6c, where there is no reduction in the amount of post-LIA mass loss shows a good fit to the RSL
534 data when the LIA termination is moved to 1800 CE, but there remains a +4 mm/yr ‘budget residual’
535 which must be accounted for from other parts of the sea-level budget. In Figure 6d, a similar good fit
536 to the RSL data is possible with a 30 % reduction in Greenland and peripheral glacier mass-loss and
537 LIA termination at 1800 CE. The remaining ‘budget residual’ is +2.5 mm/yr which again must be
538 accounted for from other parts of the sea-level budget.

539

540 The smallest calculated ‘budget residual’ ($\sim+2.5$ mm/yr) has to be found from processes causing sea-
541 level rise in southeast Greenland, such as millennial-scale Greenland GIA, Antarctic Ice Sheet melt, the
542 steric effect, and global glacier melt. The modelled sea-level budget suggests that these processes are
543 only small contributors to total sea-level change, with the sum of sources from outside Greenland only



544 +0.19 mm/yr since 1900 CE. The steric effect has the largest uncertainty, which we consider in Section
545 4.8 alongside other potential sources of error in our calculations. It is difficult however to see how the
546 contributors to RSL rise in southeast Greenland could be significantly larger before 1900 CE given the
547 cooler regional temperatures of the LIA.
548



549
550 *Figure 6. a, b) Misfit plots showing model data-fit where combinations of ‘budget residuals’ and LIA*
551 *termination dates are considered with (a) no assumed error in the RSL contribution from the GrIS and*
552 *(b) a 30 % reduction in magnitude of sea-level change associated with local changes in the GrIS. Areas*
553 *within the white lines have a statistically equivalent fit to the RSL data, c) Modelled RSL from all*
554 *combinations of LIA termination date and budget residual, assuming no error in the RSL contribution*
555 *from the GrIS. Area within the black line denotes all possible combinations of RSL trends from LIA*
556 *terminations from 1750-1900 CE and budget residual rates between 0-6mm/yr. Grey shaded area*
557 *corresponds to RSL trends from within white lines on Figure 6a, demonstrating a statistically equivalent*



558 *fit to the data. For illustrative purposes, the red line denotes a modelled RSL scenario with a budget*
559 *residual rate of +4mm/yr and LIA termination date of 1800 CE; the blue line a modelled RSL scenario*
560 *with a budget residual rate of +5mm/yr and LIA termination date of 1900 CE. d) As part c except grey*
561 *shaded area corresponds to RSL trends from Figure 6b, demonstrating a statistically equivalent fit to*
562 *the data. For illustrative purposes, the red line denotes a modelled RSL scenario with a budget residual*
563 *rate of +2.5mm/yr and LIA termination date of 1800 CE; the blue line a modelled RSL scenario with a*
564 *budget residual rate of +5mm/yr and LIA termination date of 1900 CE.*

565

566 *4.2 Reliability of saltmarsh RSL data*

567 Saltmarshes and their microfossil communities are widely used in temperate locations and previously
568 in west and south Greenland to reconstruct recent RSL changes with high precision (e.g. Kemp et al.,
569 2009, 2017; Long et al., 2012, 2010; Woodroffe and Long, 2009). At Dronning Marie Dal, the first
570 half of the RSL record (1725-1880 CE) is harder to interpret because early, rapid RSL rise may indicate
571 either a local LIA loading signal or a non RSL factor (e.g. sediment supply changes) as the marsh
572 became established. What we can say with certainty is that RSL began to fall at or soon after 1880 CE,
573 suggesting additional contributors to RSL or changes in the dominance of existing contributors caused
574 this change in the sign and rate of RSL. We are also confident of the total amount of RSL fall between
575 1880 CE and present, which is less than predicted by any permutation of the sea-level budget modelling
576 (Figure 5). We acknowledge however that these reconstructions come from a single sediment core and
577 although the stratigraphy appeared consistent across the marsh during fieldwork it would be ideal to
578 replicate these results within another core from the same marsh and also from other marshes close to
579 the ice sheet margin in this region in the future.

580

581 There is no indication of hiatuses within the marsh sediment and based on surveys of modern marshes
582 here and elsewhere in Greenland the elevation range of the key diatom species *Pinnularia intermedia*
583 used in the palaeo-marsh surface elevation calculations is robust. A RSL fall of ~0.6-0.9 m since 1900
584 CE as predicted by the sea-level budget modelling, would have lifted what was a high marsh
585 environment at the start of the period (indicated by the taxa at ~5 cm, Figure 3B) out of the intertidal
586 and into the adjacent freshwater zone where diatoms are not preserved due to extreme aridity. The



587 continuous preservation of intertidal diatoms through the sediment sequence to the surface where
588 modern saltmarsh plants were growing during sampling (Figure 2) rules out this possibility. Even the
589 smaller amount of RSL fall (~0.2 m) since 1900 CE predicted by an earlier LIA termination date (1800
590 CE) and 30% smaller GrIS contribution (Figure 6) is unlikely because the diatoms suggest a mid-high
591 marsh environment at 1900 CE and the core top elevation is within the high marsh zone, a vertical
592 distance based on analysis of modern diatoms at Dronning Marie Dal of ~0.1 m, which is half of the
593 predicted RSL fall (~0.2 m). Greenland saltmarshes accrete very slowly and only record sustained RSL
594 changes over decades, and therefore short-timescale variability in contributors (e.g. due to decadal
595 temperature fluctuations in the 20th Century) is not distinguishable in the saltmarsh data. However, the
596 total amount of RSL fall and the timing of the change from RSL rise/stability to RSL fall is robustly
597 reconstructed and we are confident that this provides an important test of Greenland RSL modelling.

598

599 *4.3 Limitations of RSL modelling*

600 Regional sea level budgets deviate significantly from the global budget, are challenging to compute and
601 have been deemed part of the ‘Regional Sea-Level Change and Coastal Impacts’ Grand Challenge by
602 the World Climate Research Programme (WCRP, 2022). Of the different items in the sea-level budget
603 for Dronning Marie Dal, the large uncertainty in the steric contribution could potentially be the source
604 of additional sea-level rise which would help decrease the ‘budget residual’ identified in Figure 6. The
605 data in Table 4 do not fully capture the range of uncertainty in the steric component of sea level. These
606 uncertainties arise from poor to non-existent capture of the dynamics of coastal regions, namely the
607 propagation of the change in steric height of the open ocean to the fjord location and the lack of
608 observations to constrain model output in the early 20th Century.

609

610 The field site is located at the head of the 50 km long marine fjord Søndre Skoldungesund and therefore
611 the steric contribution may be different to that calculated from the open ocean estimates within 300 km
612 of Dronning Marie Dal averaged in this study. A multibeam study of the fjord by Kjeldsen et al. (2017)
613 shows the fjord is between 1.1-3.1 km wide, up to 800 m deep in the outer part, with a shallow (77m
614 deep) sill at mid-fjord and shallow depths inside the sill. The fjord water is cold to the base along its
615 length, with no apparent intrusion of warmer Atlantic water from the shelf edge. The mixed predictions



616 of steric height changes from the different models suggest that this region is poorly constrained within
617 global steric datasets (Table 4). Given the lack of intrusion of warm Atlantic water into the fjord today
618 it is unlikely that there has been a more positive contribution of steric height from 20th Century warming.
619 However, with significant mass loss from the Greenland Ice Sheet since the LIA and an influx of cold
620 yet low-salinity meltwater into the fjord it is possible that the local halosteric component is
621 underestimated.

622

623 A second issue with the steric height calculation is the potential for the CMIP6 models to misrepresent
624 changes in the dynamic height of the ocean caused by shifts in the location of ocean currents, such as
625 the East Greenland Current (EGC) over time. A recent study of North Atlantic dynamic sea level and
626 its response to GrIS meltwater and temperature increase indicates general Atlantic Meridional
627 Overturning Circulation decline and increase in sea-surface height with increased GrIS melting, but the
628 response of the cold EGC is complex and in southeast Greenland the effect of warming and increased
629 meltwater on sea-surface height is minimal (Saenko et al., 2017). Given that Kjeldsen et al. (2017)
630 suggest the EGC does not currently penetrate into the Søndre Skoldungesund fjord the impact of any
631 dynamical changes in the EGC since the LIA are likely to be minor.

632

633 A third possible source of uncertainty in the sea-level budget is the application of the sea level code
634 used to calculate GIA, specifically the spectral resolution with which the algorithm predicts the sea
635 level response to loading increments. The mass balance history from Kjeldsen et al. (2015) is presented
636 on a 1x1 km spatial grid, but the sea level code utilises a spectral harmonic truncation of 256. The
637 effects on predicted RSL of the reduction in resolution has been demonstrated previously with near-
638 field relative sea level being more affected by harmonic truncation than far field sites (Spada and Melini,
639 2019). A move towards a higher degree spherical harmonic truncation (>1024) would be necessary to
640 faithfully reproduce sea level fingerprint histories associated with small outlet glaciers and should be
641 considered in the future (Adhikari et al., 2015).

642

643 Despite the limitations outlined above, this study presents a first test of a post-LIA sea-level budget in
644 the nearfield location of southeast Greenland. There is clear and unexplained difference between the



645 RSL history recorded by salt marsh sediments (a small RSL fall since the end of the LIA) and the RSL
646 budget which suggests significant RSL fall during this period. The sensitivity tests show that the budget
647 can fit the salt marsh RSL data if the amount of mass loss from the GrIS and peripheral glaciers is less,
648 and it took place over a longer period (Figure 6d), but even so a +2.5 mm/yr unexplained ‘budget
649 residual’ remains. RSL reconstructions from salt marshes in southwest Greenland (Long et al., 2012,
650 2010; Woodroffe and Long, 2010, 2009) also suggest that the dominant signal in southern Greenland is
651 RSL rise into the 20th Century, which correlates with the long term (pre ~1880 CE) trend of RSL rise at
652 Dronning Marie Dal.

653

654 **5. Conclusions**

655 Saltmarsh sediments collected at the mouth of Dronning Marie Dal, close to the GrIS margin in
656 southeast Greenland, record RSL changes over the past c. 300 years in changing sediment and diatom
657 stratigraphy. These RSL changes record a combination of processes that are dominated by
658 local/regional changes in GrIS mass balance during this critical period that spans the maximum of the
659 LIA and 20th Century warming.

660

661 In the early part of the record (1725-1762 CE) the rate of RSL rise is higher than reconstructed from
662 the closest isolation basin at Timmiarmiut, but between 1762-1880 CE the rate decreases to within the
663 error range of the isolation basin RSL rate. This trend is likely due to changes in the local LIA ice load
664 over this time period combined with ongoing millennial-scale GIA, or other local processes as the salt
665 marsh is established. Other recent estimates of centennial-scale GIA (Khan et al., 2016; van Dam et
666 al., 2017) suggest that RSL should have been falling over the past few hundred years at Dronning Marie
667 Dal. The isolation basin and salt marsh data instead suggest that RSL was rising or close to stable from
668 c. 1100 CE until c. 1880 CE. RSL begins to slowly fall around 1880 CE and the rate then accelerates
669 from the 1990s, with a total amount of RSL fall of 0.08 ± 0.1 m since 1880 CE.

670

671

672



673 Modelled RSL, which takes into account contributions from post-LIA GrIS GIA, ongoing deglacial
674 GIA, the global non-ice sheet glacial fingerprint, the contribution from thermosteric effects, an estimate
675 of the Antarctic fingerprint and the contribution from terrestrial water storage, over-predicts the amount
676 of RSL fall since the end of the LIA by at least 0.5 m. The GIA signal caused by post-LIA GrIS mass
677 loss is by far the largest contributor, and error in its calculation has the largest potential to impact RSL
678 predictions at Dronning Marie Dal. We cannot reconcile the modelled contributions and the saltmarsh
679 observations, even when moving the termination of the LIA to 1800 CE, and reducing the post-LIA
680 Greenland mass loss signal by 30%. A ‘budget residual’ of $\sim +2.5$ mm/yr since the end of the LIA
681 remains unexplained. Explaining the difference between salt marsh RSL data and the modelled RSL
682 budget since the end of the LIA should be a key future research objective through reducing uncertainty
683 on each component to the sea-level budget, collecting more empirical data on the recent history of the
684 GrIS and by replicating the salt marsh RSL record presented here elsewhere in this and other regions of
685 Greenland.

686

687 *Author Contribution*

688 SAW, LMW, AJL and KKK designed the study, SAW, KKK and KHK undertook fieldwork, NLMB
689 undertook the laboratory analysis, and SAW and LMW prepared the manuscript with contributions
690 from all co-authors.

691

692 The authors declare that they have no conflict of interest.

693

694 *Acknowledgements*

695 We acknowledge funding from Danish Agency for Science, Technology and Innovation, ‘Greenland
696 ice sheet over the past millennium’ (PI Kurt Kjær) and the assistance of the captain and crew onboard
697 SS ACTIV for their help collecting the data during the field campaign to southeast Greenland. Barlow’s
698 postdoctoral position to undertake this work was funded by Durham University Department of
699 Geography. We thank the laboratory technicians within Durham Geography for their support with
700 sample preparation. The authors acknowledge the International Union for Quaternary Sciences
701 (INQUA) Coastal and Marine Processes (CMP) Commission and PALSEA, a working group of INQUA



- 702 and Past Global Changes (PAGES), which in turn receives support from the Swiss Academy of Sciences
703 and the Chinese Academy of Sciences.
704
- 705 Adhikari, S., Ivins, E. R., and Larour, E.: ISSM-SESAW v1.0: mesh-based computation of
706 gravitationally consistent sea level and geodetic signatures caused by cryosphere and
707 climate driven mass change, *Climate and Earth System Modeling*,
708 <https://doi.org/10.5194/gmdd-8-9769-2015>, 2015.
- 709 Adhikari, S., Caron, L., Steinberger, B., Reager, J. T., Kjeldsen, K. K., Marzeion, B., Larour,
710 E., and Ivins, E. R.: What drives 20th century polar motion?, *Earth Planet. Sci. Lett.*, 502,
711 126–132, <https://doi.org/10.1016/j.epsl.2018.08.059>, 2018.
- 712 Adhikari, S., Milne, G. A., Caron, L., Khan, S. A., Kjeldsen, K. K., Nilsson, J., Larour, E., and
713 Ivins, E. R.: Decadal to Centennial Timescale Mantle Viscosity Inferred from Modern Crustal
714 Uplift Rates in Greenland, *Geophys. Res. Lett.*, n/a, e2021GL094040,
715 <https://doi.org/10.1029/2021GL094040>, 2021.
- 716 Allen, J. R. L.: Morphodynamics of Holocene salt marshes: a review sketch from the Atlantic
717 and Southern North Sea coasts of Europe, *Quat. Sci. Rev.*, 19, 1155–1231,
718 [https://doi.org/10.1016/S0277-3791\(99\)00034-7](https://doi.org/10.1016/S0277-3791(99)00034-7), 2000.
- 719 Bamber, J. and Riva, R.: The sea level fingerprint of recent ice mass fluxes, *The*
720 *Cryosphere*, 4, 621–627, <https://doi.org/10.5194/tc-4-621-2010>, 2010.
- 721 Barlow, N. L. M., Shennan, I., Long, A. J., Gehrels, W. R., Saher, M. H., Woodroffe, S. A.,
722 and Hillier, C.: Salt marshes as late Holocene tide gauges, *Glob. Planet. Change*, 106, 90–
723 110, <https://doi.org/10.1016/j.gloplacha.2013.03.003>, 2013.
- 724 Bevis, M., Wahr, J., Khan, S. A., Madsen, F. B., Brown, A., Willis, M., Kendrick, E., Knudsen,
725 P., Box, J. E., van Dam, T., Caccamise, D. J., Johns, B., Nylén, T., Abbott, R., White, S.,
726 Miner, J., Forsberg, R., Zhou, H., Wang, J., Wilson, T., Bromwich, D., and Francis, O.:
727 Bedrock displacements in Greenland manifest ice mass variations, climate cycles and
728 climate change, *Proc. Natl. Acad. Sci. U. S. A.*, 109, 11944–11948, <https://doi.org/10.1073/pnas.1204664109>, 2012.
- 730 Bevis, M., Harig, C., Khan, S. A., Brown, A., Simons, F. J., Willis, M., Fettweis, X., Broeke,
731 M. R. van den, Madsen, F. B., Kendrick, E., Caccamise, D. J., Dam, T. van, Knudsen, P.,
732 and Nylén, T.: Accelerating changes in ice mass within Greenland, and the ice sheet's
733 sensitivity to atmospheric forcing, *Proc. Natl. Acad. Sci.*, 116, 1934–1939,
734 <https://doi.org/10.1073/pnas.1806562116>, 2019.
- 735 Bindler, R., Renberg, I., Appleby, P. G., Anderson, N. J., and Rose, N. L.: Mercury
736 Accumulation Rates and Spatial Patterns in Lake Sediments from West Greenland: A Coast
737 to Ice Margin Transect, *Environ. Sci. Technol.*, 35, 1736–1741,
738 <https://doi.org/10.1021/es0002868>, 2001.
- 739 Björk, A. A., Kjaer, K. H., Korsgaard, N. J., Khan, S. A., Kjeldsen, K. K., Andresen, C. S.,
740 Box, J. E., Larsen, N. K., and Funder, S.: An aerial view of 80 years of climate-related glacier
741 fluctuations in southeast Greenland, *Nat. Geosci.*, 5, 427–432,
742 <https://doi.org/10.1038/Ngeo1481>, 2012.
- 743 Briner, J. P., Young, N. E., Thomas, E. K., Stewart, H. A. M., Losee, S., and Truex, S.: Varve
744 and radiocarbon dating support the rapid advance of Jakobshavn Isbræ during the Little Ice
745 Age, *Quat. Sci. Rev.*, 30, 2476–2486, <https://doi.org/10.1016/j.quascirev.2011.05.017>, 2011.



- 746 Briner, J. P., Cuzzzone, J. K., Badgley, J. A., Young, N. E., Steig, E. J., Morlighem, M.,
747 Schlegel, N.-J., Hakim, G. J., Schaefer, J. M., Johnson, J. V., Lesnek, A. J., Thomas, E. K.,
748 Allan, E., Bennike, O., Cluett, A. A., Csatho, B., de Vernal, A., Downs, J., Larour, E., and
749 Nowicki, S.: Rate of mass loss from the Greenland Ice Sheet will exceed Holocene values
750 this century, *Nature*, 586, 70–74, <https://doi.org/10.1038/s41586-020-2742-6>, 2020.
- 751 van den Broeke, M., Bamber, J., Ettema, J., Rignot, E., Schrama, E., van de Berg, W., van
752 Meijgaard, E., Velicogna, I., and Wouters, B.: Partitioning Recent Greenland Mass Loss,
753 *Science*, 326, 984–986, <https://doi.org/10.1126/science.1178176>, 2009.
- 754 Bronk Ramsey, C.: Bayesian analysis of radiocarbon dates, *Radiocarbon*, 51, 337–360,
755 2009.
- 756 Chao, B. F., Wu, Y. H., and Li, Y. S.: Impact of Artificial Reservoir Water Impoundment on
757 Global Sea Level, *Science*, 320, 212–214, <https://doi.org/10.1126/science.1154580>, 2008.
- 758 Chen, G., Zhang, S., Liang, S., and Zhu, J.: Elevation and Volume Changes in Greenland
759 Ice Sheet From 2010 to 2019 Derived From Altimetry Data, *Front. Earth Sci.*, 9, 674983,
760 <https://doi.org/10.3389/feart.2021.674983>, 2021.
- 761 Chylek, P., Dubey, M. K., and Lesins, G.: Greenland warming of 1920-1930 and 1995-2005,
762 *Geophys. Res. Lett.*, 33, <https://doi.org/Artn L11707> 10.1029/2006gl026510, 2006.
- 763 van Dam, T., Francis, O., Wahr, J., Khan, S. A., Bevis, M., and van den Broeke, M. R.: Using
764 GPS and absolute gravity observations to separate the effects of present-day and
765 Pleistocene ice-mass changes in South East Greenland, *Earth Planet. Sci. Lett.*, 459, 127–
766 135, <https://doi.org/10.1016/j.epsl.2016.11.014>, 2017.
- 767 Döll, P., Müller Schmied, H., Schuh, C., Portmann, F. T., and Eicker, A.: Global-scale
768 assessment of groundwater depletion and related groundwater abstractions: Combining
769 hydrological modeling with information from well observations and GRACE satellites, *Water
770 Resour. Res.*, 50, 5698–5720, <https://doi.org/10.1002/2014WR015595>, 2014.
- 771 Dyke, L. M., Hughes, A. L. C., Murray, T., Hiemstra, J. F., Andresen, C. S., and Rodés, Á.:
772 Evidence for the asynchronous retreat of large outlet glaciers in southeast Greenland at the
773 end of the last glaciation, *Quat. Sci. Rev.*, 99, 244–259,
774 <https://doi.org/10.1016/j.quascirev.2014.06.001>, 2014.
- 775 Dyke, L. M., Hughes, A. L., Andresen, C. S., Murray, T., Hiemstra, J. F., Bjørk, A. A., and
776 Rodés, Á.: The deglaciation of coastal areas of southeast Greenland, *The Holocene*, 28,
777 1535–1544, <https://doi.org/10.1177/0959683618777067>, 2018.
- 778 Dziewonski, A. M. and Anderson, D. L.: Preliminary reference Earth model, *Phys. Earth
779 Planet. Inter.*, 25, 297–356, [https://doi.org/10.1016/0031-9201\(81\)90046-7](https://doi.org/10.1016/0031-9201(81)90046-7), 1981.
- 780 Eyring, V., Bony, S., Meehl, G. A., Senior, C. A., Stevens, B., Stouffer, R. J., and Taylor, K.
781 E.: Overview of the Coupled Model Intercomparison Project Phase 6 (CMIP6) experimental
782 design and organization, *Geosci. Model Dev.*, 9, 1937–1958, [https://doi.org/10.5194/gmd-9-
783 1937-2016](https://doi.org/10.5194/gmd-9-1937-2016), 2016.
- 784 Farrell, W. E. and Clark, J. A.: On Postglacial Sea Level, *Geophys. J. R. Astron. Soc.*, 46,
785 647–667, <https://doi.org/10.1111/j.1365-246X.1976.tb01252.x>, 1976.
- 786 Frederikse, T., Landerer, F., Caron, L., Adhikari, S., Parkes, D., Humphrey, V. W.,
787 Dangendorf, S., Hogarth, P., Zanna, L., Cheng, L., and Wu, Y.-H.: The causes of sea-level
788 rise since 1900, *Nature*, 584, 393–397, <https://doi.org/10.1038/s41586-020-2591-3>, 2020.



- 789 Funder, S. and Hansen, L.: The Greenland ice sheet - a model for its culmination and decay
790 during and after the last glacial maximum, *Bull. Geol. Soc. Den.*, 42, 137–152, 1996.
- 791 Funder, S., Kjeldsen, K. K., Kjaer, K. H., and O Cofaigh, C.: The Greenland Ice Sheet during
792 the last 300,000 years: a review, *Dev. Quat. Sci.*, 15, 699-713. doi: 10.1016/B978-0-444-
793 53447-7.00050-7, 2011.
- 794 Hughes, A., Rainsley, E., Murray, T., Fogwill, C., Schnabel, C., and Xu, S.: Rapid response
795 of Helheim Glacier, southeast Greenland, to early Holocene climate warming, *Geology*, 40,
796 427–430, <https://doi.org/10.1130/G32730.1>, 2012.
- 797 Humphrey, V. and Gudmundsson, L.: GRACE-REC: a reconstruction of climate-driven water
798 storage changes over the last century, *Earth Syst. Sci. Data*, 11, 1153–1170,
799 <https://doi.org/10.5194/essd-11-1153-2019>, 2019.
- 800 Ivchenko, V. O., Danilov, S., Sidorenko, D., Schröter, J., Wenzel, M., and Aleynik, D. L.:
801 Steric height variability in the Northern Atlantic on seasonal and interannual scales, *J.*
802 *Geophys. Res.*, 113, C11007, <https://doi.org/10.1029/2008JC004836>, 2008.
- 803 Kemp, A., Horton, B., Culver, S., Corbett, D., van de Plassche, O., Gehrels, W., Douglas, B.,
804 and Parnell, A.: Timing and magnitude of recent accelerated sea-level rise (North Carolina,
805 United States), *Geology*, 37, 1035–1038, <https://doi.org/10.1130/G30352A.1>, 2009.
- 806 Kemp, A. C., Kegel, J. J., Culver, S. J., Barber, D. C., Mallinson, D. J., Leorri, E., Bernhardt,
807 C. E., Cahill, N., Riggs, S. R., Woodson, A. L., Mulligan, R. P., and Horton, B. P.: Extended
808 late Holocene relative sea-level histories for North Carolina, USA, *Quat. Sci. Rev.*, 160, 13–
809 30, <https://doi.org/10.1016/j.quascirev.2017.01.012>, 2017.
- 810 Kendall, R. A., Mitrovica, J. X., and Milne, G. A.: On post-glacial sea level - II. Numerical
811 formulation and comparative results on spherically symmetric models, *Geophys. J. Int.*, 161,
812 679–706, <https://doi.org/10.1111/j.1365-246X.2005.02553.x>, 2005.
- 813 Khan, S. A., Aschwanden, A., Bjork, A. A., Wahr, J., Kjeldsen, K. K., and Kjaer, K. H.:
814 Greenland ice sheet mass balance: a review, *Rep. Prog. Phys.*, 78, 26,
815 <https://doi.org/10.1088/0034-4885/78/4/046801>, 2015.
- 816 Khan, S. A., Sasgen, I., Bevis, M., van Dam, T., Bamber, J. L., Wahr, J., Willis, M., Kjaer, K.
817 H., Wouters, B., Helm, V., Csatho, B., Fleming, K., Bjork, A. A., Aschwanden, A., Knudsen,
818 P., and Munneke, P. K.: Geodetic measurements reveal similarities between post-Last
819 Glacial Maximum and present-day mass loss from the Greenland ice sheet, *Sci. Adv.*, 2,
820 <https://doi.org/ARTN e1600931> 10.1126/sciadv.1600931, 2016.
- 821 Khan, S. A., Bjørk, A. A., Bamber, J. L., Morlighem, M., Bevis, M., Kjær, K. H., Mouginit, J.,
822 Løkkegaard, A., Holland, D. M., Aschwanden, A., Zhang, B., Helm, V., Korsgaard, N. J.,
823 Colgan, W., Larsen, N. K., Liu, L., Hansen, K., Barletta, V., Dahl-Jensen, T. S.,
824 Søndergaard, A. S., Csatho, B. M., Sasgen, I., Box, J., and Schenk, T.: Centennial response
825 of Greenland's three largest outlet glaciers, *Nat. Commun.*, 11, 5718,
826 <https://doi.org/10.1038/s41467-020-19580-5>, 2020.
- 827 Kjær, K. H., Bjørk, A. A., Kjeldsen, K. K., Hansen, E. S., Andresen, C. S., Siggaard-
828 Andersen, M.-L., Khan, S. A., Søndergaard, A. S., Colgan, W., Schomacker, A., Woodroffe,
829 S., Funder, S., Rouillard, A., Jensen, J. F., and Larsen, N. K.: Glacier response to the Little
830 Ice Age during the Neoglacial cooling in Greenland, *Earth-Sci. Rev.*, 227, 103984,
831 <https://doi.org/10.1016/j.earscirev.2022.103984>, 2022.
- 832 Kjeldsen, K., Korsgaard, N., Bjork, A., Khan, S., Box, J., Funder, S., Larsen, N., Bamber, J.,
833 Colgan, W., van den Broeke, M., Siggaard-Andersen, M., Nuth, C., Schomacker, A.,
834 Andresen, C., Willerslev, E., and Kjaer, K.: Spatial and temporal distribution of mass loss



- 835 from the Greenland Ice Sheet since AD 1900, *Nature*, 528, 396–400,
836 <https://doi.org/10.1038/nature16183>, 2015.
- 837 Kjeldsen, K. K., Weinrebe, R. W., Bendtsen, J., Bjørk, A. A., and Kjær, K. H.: Multibeam
838 bathymetry and CTD measurements in two fjord systems in southeastern Greenland, *Earth
839 Syst. Sci. Data*, 9, 589–600, <https://doi.org/10.5194/essd-9-589-2017>, 2017.
- 840 Lecavalier, B., Milne, G. A., Simpson, M. J. R., Wake, L. M., Huybrechts, P., Tarasov, L.,
841 Kjeldsen, K. K., Funder, S. V., Long, A. J., Woodroffe, S. A., Dyke, A., and Larsen, N. K.: A
842 model of Greenland ice sheet deglaciation based on observations of relative sea-level and
843 ice extent, *Quat. Sci. Rev.*, in press, 2014.
- 844 Lepping, O. and Daniëls, F. J. A.: Phytosociology of Beach and Salt Marsh Vegetation in
845 Northern West Greenland, *Polarforschung*, 76, 95–108, 2007.
- 846 Levy, L. B., Larsen, N. K., Knudsen, M. F., Egholm, D. L., Bjørk, A. A., Kjeldsen, K. K., Kelly,
847 M. A., Howley, J. A., Olsen, J., Tikhomirov, D., Zimmerman, S. R. H., and Kjær, K. H.: Multi-
848 phased deglaciation of south and southeast Greenland controlled by climate and
849 topographic setting, *Quat. Sci. Rev.*, 242, 106454,
850 <https://doi.org/10.1016/j.quascirev.2020.106454>, 2020.
- 851 Lindeberg, C., Bindler, R., Renberg, I., Emteryd, O., Karlsson, E., and Anderson, N. J.:
852 Natural Fluctuations of Mercury and Lead in Greenland Lake Sediments, *Environ. Sci.
853 Technol.*, 40, 90–95, <https://doi.org/10.1021/es051223y>, 2006.
- 854 Long, A. J., Woodroffe, S. A., Milne, G. A., Bryant, C. L., and Wake, L. M.: Relative sea-level
855 change in West Greenland during the last millennium, *Quat. Sci. Rev.*, 29, 367–383, 2010.
- 856 Long, A. J., Woodroffe, S. A., Milne, G. A., Bryant, C. L., Simpson, M. J. R., and Wake, L.
857 M.: Relative sea-level change in Greenland during the last 700 yrs and ice sheet response to
858 the Little Ice Age, *Earth Planet. Sci. Lett.*, 315, 76–85, <https://doi.org/DOI>
859 [10.1016/j.epsl.2011.06.027](https://doi.org/10.1016/j.epsl.2011.06.027), 2012.
- 860 Marzeion, B., Jarosch, A. H., and Hofer, M.: Past and future sea-level change from the
861 surface mass balance of glaciers, *The Cryosphere*, 6, 1295–1322, [https://doi.org/10.5194/tc-](https://doi.org/10.5194/tc-6-1295-2012)
862 [6-1295-2012](https://doi.org/10.5194/tc-6-1295-2012), 2012.
- 863 Marzeion, B., Leclercq, P. W., Cogley, J. G., and Jarosch, A. H.: Brief Communication:
864 Global reconstructions of glacier mass change during the 20th century are consistent, *The
865 Cryosphere*, 9, 2399–2404, <https://doi.org/10.5194/tc-9-2399-2015>, 2015.
- 866 McDougall, T. J. and Barker, P. M.: Getting started with TEOS-10 and the Gibbs Seawater
867 (GSW) Oceanographic Toolbox., 2011.
- 868 Meredith, M., Sommerkorn, M., Cassotta, S., Derksen, C., Ekaykin, A., Hollowed, A.,
869 Kofinas, G., Mackintosh, A., Melbourne-Thomas, J., Muelbert, M. M. C., Ottersen, G.,
870 Pritchard, H., and Schuur, E. A. G.: Polar Regions, in: IPCC Special Report on the Ocean
871 and Cryosphere in a Changing Climate, Cambridge University Press, 203–320, 2019.
- 872 Mitrovica, J. X. and Milne, G. A.: On post-glacial sea level: I. General theory, *Geophys. J.
873 Int.*, 154, 253–267, <https://doi.org/DOI> [10.1046/j.1365-246X.2003.01942.x](https://doi.org/10.1046/j.1365-246X.2003.01942.x), 2003.
- 874 Mitrovica, J. X., Tamisiea, M. E., Davis, J. L., and Milne, G. A.: Recent mass balance of
875 polar ice sheets inferred from patterns of global sea-level change, *Nature*, 409, 1026–1029,
876 <https://doi.org/10.1038/35059054>, 2001.
- 877 Moon, T., Joughin, I., Smith, B., and Howat, I.: 21st-Century Evolution of Greenland Outlet
878 Glacier Velocities, *Science*, 336, 576–578, <https://doi.org/10.1126/science.1219985>, 2012.



- 879 Morlighem, M., Williams, C. N., Rignot, E., An, L., Arndt, J. E., Bamber, J. L., Catania, G.,
880 Chauché, N., Dowdeswell, J. A., Dorschel, B., Fenty, I., Hogan, K., Howat, I., Hubbard, A.,
881 Jakobsson, M., Jordan, T. M., Kjeldsen, K. K., Millan, R., Mayer, L., Mouginot, J., Noël, B. P.
882 Y., O’Cofaigh, C., Palmer, S., Rysgaard, S., Seroussi, H., Siegert, M. J., Slabon, P., Straneo,
883 F., van den Broeke, M. R., Weinrebe, W., Wood, M., and Zinglensen, K. B.: BedMachine v3:
884 Complete Bed Topography and Ocean Bathymetry Mapping of Greenland From Multibeam
885 Echo Sounding Combined With Mass Conservation, *Geophys. Res. Lett.*, 44, 11,051-
886 11,061, <https://doi.org/10.1002/2017GL074954>, 2017.
- 887 Pérez-Rodríguez, M., Silva-Sánchez, N., Kylander, M. E., Bindler, R., Mighall, T. M.,
888 Schofield, J. E., Edwards, K. J., and Martínez Cortizas, A.: Industrial-era lead and mercury
889 contamination in southern Greenland implicates North American sources, *Sci. Total*
890 *Environ.*, 613–614, 919–930, <https://doi.org/10.1016/j.scitotenv.2017.09.041>, 2018.
- 891 Pritchard, H., Arthern, R., Vaughan, D., and Edwards, L.: Extensive dynamic thinning on the
892 margins of the Greenland and Antarctic ice sheets, *Nature*, 461, 971–975,
893 <https://doi.org/10.1038/nature08471>, 2009.
- 894 Ramsey, C. B. and Lee, S.: Recent and Planned Developments of the Program OxCal,
895 *Radiocarbon*, 55, 720–730, <https://doi.org/10.1017/S0033822200057878>, 2013.
- 896 Reimer, P. J., Austin, W. E. N., Bard, E., Bayliss, A., Blackwell, P. G., Ramsey, C. B., Butzin,
897 M., Cheng, H., Edwards, R. L., Friedrich, M., Grootes, P. M., Guilderson, T. P., Hajdas, I.,
898 Heaton, T. J., Hogg, A. G., Hughen, K. A., Kromer, B., Manning, S. W., Muscheler, R.,
899 Palmer, J. G., Pearson, C., Plicht, J. van der, Reimer, R. W., Richards, D. A., Scott, E. M.,
900 Southon, J. R., Turney, C. S. M., Wacker, L., Adolphi, F., Büntgen, U., Capano, M., Fahrni,
901 S. M., Fogtmann-Schulz, A., Friedrich, R., Köhler, P., Kudsk, S., Miyake, F., Olsen, J.,
902 Reinig, F., Sakamoto, M., Sookdeo, A., and Talamo, S.: The IntCal20 Northern Hemisphere
903 Radiocarbon Age Calibration Curve (0–55 cal kBP), *Radiocarbon*, 62, 725–757,
904 <https://doi.org/10.1017/RDC.2020.41>, 2020.
- 905 Richter, A., Rysgaard, S., Dietrich, R., Mortensen, J., and Petersen, D.: Coastal tides in
906 West Greenland derived from tide gauge records, *Ocean Dyn.*, 61, 39–49,
907 <https://doi.org/10.1007/s10236-010-0341-z>, 2011.
- 908 Saenko, O. A., Yang, D., and Myers, P. G.: Response of the North Atlantic dynamic sea
909 level and circulation to Greenland meltwater and climate change in an eddy-permitting ocean
910 model, *Clim. Dyn.*, 49, 2895–2910, <https://doi.org/10.1007/s00382-016-3495-7>, 2017.
- 911 Shotyk, W., Goodsite, M. E., Roos-Barracough, F., Frei, R., Heinemeier, J., Asmund, G.,
912 Lohse, C., and Hansen, T. S.: Anthropogenic contributions to atmospheric Hg, Pb and As
913 accumulation recorded by peat cores from southern Greenland and Denmark dated using
914 the 14C “bomb pulse curve,” *Geochim. Cosmochim. Acta*, 67, 3991–4011,
915 [https://doi.org/10.1016/S0016-7037\(03\)00409-5](https://doi.org/10.1016/S0016-7037(03)00409-5), 2003.
- 916 Spada, G. and Melini, D.: SELEN4; (SELEN version 4.0): a Fortran program for solving the
917 gravitationally and topographically self-consistent sea-level equation in glacial isostatic
918 adjustment modeling, *Geosci. Model Dev.*, 12, 5055–5075, <https://doi.org/10.5194/gmd-12-5055-2019>, 2019.
- 920 The IMBIE Team: Mass balance of the Greenland Ice Sheet from 1992 to 2018, *Nature*, 579,
921 233–239, <https://doi.org/10.1038/s41586-019-1855-2>, 2020.
- 922 Vogt, T.: Late-Quaternary Oscillations of Level in Southeast Greenland., Oslo: Dybwad
923 1933., 44 pp., 1933.



- 924 Wada, Y., Lo, M.-H., Yeh, P. J.-F., Reager, J. T., Famiglietti, J. S., Wu, R.-J., and Tseng, Y.-
925 H.: Fate of water pumped from underground and contributions to sea-level rise, *Nat. Clim.*
926 *Change*, 6, 777–780, <https://doi.org/10.1038/nclimate3001>, 2016.
- 927 Wangner, D. J., Sicre, M., Kjeldsen, K. K., Jaeger, J. M., Bjørk, A. A., Vermassen, F., Sha,
928 L., Kjær, K. H., Klein, V., and Andresen, C. S.: Sea Surface Temperature Variability on the
929 SE-Greenland Shelf (1796–2013 CE) and Its Influence on Thrym Glacier in Nørre
930 Skjoldungesund, *Paleoceanogr. Paleoclimatology*, 35,
931 <https://doi.org/10.1029/2019PA003692>, 2020.
- 932 Wood, K. R. and Overland, J. E.: Early 20th century Arctic warming in retrospect, *Int. J.*
933 *Climatol.*, 30, 1269–1279, <https://doi.org/10.1002/joc.1973>, 2010.
- 934 Woodroffe, S. A. and Long, A. J.: Salt marshes as archives of recent relative sea-level
935 change in West Greenland, *Quat. Sci. Rev.*, 28, 1750–1761, 2009.
- 936 Woodroffe, S. A. and Long, A. J.: Reconstructing recent relative sea-level changes in West
937 Greenland: local diatom-based transfer functions are superior to regional models, *Quat. Int.*,
938 221, 91–103, 2010.
- 939 Zheng, J.: Archives of total mercury reconstructed with ice and snow from Greenland and
940 the Canadian High Arctic, *Sci. Total Environ.*, 509–510, 133–144,
941 <https://doi.org/10.1016/j.scitotenv.2014.05.078>, 2015.

942

943

944